Sensitivity Analysis of Launch Activities in Low Earth Orbit

Gian Luigi Somma [1*], Hugh G. Lewis [2], Camilla Colombo [3]

[1] Faculty of Engineering and the Environment, University of Southampton, United Kingdom, email: GL.Somma@soton.ac.uk

[2] Faculty of Engineering and the Environment, University of Southampton, United Kingdom, email: H.G.Lewis@soton.ac.uk

[3] Department of Aerospace Science and Technology, Politecnico di Milano, Italia, email: camilla.colombo@polimi.it

[*] Corresponding author

DOI: 10.1016/j.actaastro.2018.05.043

Abstract

This work aims to investigate the response of the low Earth orbit environment to the change in number and distribution of new launches and to understand the effects of the size and post-mission lifetime of a large constellation of spacecraft. The analysis presented in this paper were carried out using MISSD, Model to Investigate control Strategies for Space Debris, a multi-shell, and multi-species source-sink statistical model able to simulate the injection, removal and interaction of six type of objects up to an altitude of 2000 km. The results suggest that multiple regions experience a sensible increment in the orbital density when slightly increasing the launch activity for the next 200 years. Recently, many private companies expressed their interest in putting large constellations of satellites at 1100-1300 km altitude. However, results show that the launch of just six additional spacecraft per year in this region increased the spatial density by an amount equal to the projection over 200 years of today's most crowded region.

Results also show that the increase in the orbital population and collision risk caused by the presence of large constellations could be mitigated using a high level of post-mission disposal compliance, reliable deorbit mechanisms and reducing the post-mission lifetime to 5 years.

Keywords: space debris, low Earth orbit, sensitivity analysis, satellite constellations, space sustainability

1 Introduction

Space debris models are based on several hypotheses, some of which can influence the model behaviours and their results. Sometimes even a change of few percentage points in the simulation variables (such as a different distribution in the initial population, launch activity, atmospheric model, objects radius and mass, break-up models and collision probability estimation) can lead to significant variation in the evolution of the orbital population [1,2]. Moreover, some simulation variables have a significant uncertainty (e.g. the uncatalogued space debris population and the objects' cross-sectional areas) or just cannot be accurately predicted by their nature of future events (e.g. the solar activity) [2]. Some of these variables, mostly linked to physical parameters or behaviours, can be improved at least partially by increasing our knowledge of the subject. For example, the solar and the atmospheric density models can be revised to enhance (but not to completely forecast) the solar activity and re-entry predictions, or more observing campaigns can be performed to increase the accuracy of the actual debris population. A second group of variables relates directly to the simulation hypothesis and are, for example, the future launch rate and altitude profile, the satellite operational life, the Post Mission Disposal (PMD) compliance level and their residual orbital lifetime (i.e. the time needed by the object to re-enter the atmosphere after the end of the mission).

This work aims to investigate the influence of different launch rates and profiles in the Low Earth Orbit (LEO) region to understand their long-term effect on the evolution of the orbital population. The focus on various launch rates is also of interest considering recent proposals by several private companies (e.g. Boeing, OneWeb, Planet Labs, Samsung, SpaceX) to deploy so-called large and "mega constellations" [3–5]. Therefore, different launch rates and distributions may simulate the build-up and the replenishment of such orbital constellations. Finally, the size of these constellations and the orbital lifetime of each satellite composing them

is considered, to study the influence of the constellation presence on the orbital population and collision risk.

2 MISSD: a Model to Investigate control Strategies for Space Debris

The analyses presented in this paper were carried out using MISSD (Model to Investigate control Strategies for Space Debris), a source-sink statistical model for the LEO region developed at the University of Southampton [6,7]. MISSD is a multi-shell, multi-species model able to simulate object injection and removal from a custom number of spherical altitude shells around the Earth, from 200 to 2000 km. Figure 1 depicts the model schematics, with inbound and outbound arrows representing the addition or removal of objects from each of the six species implemented.

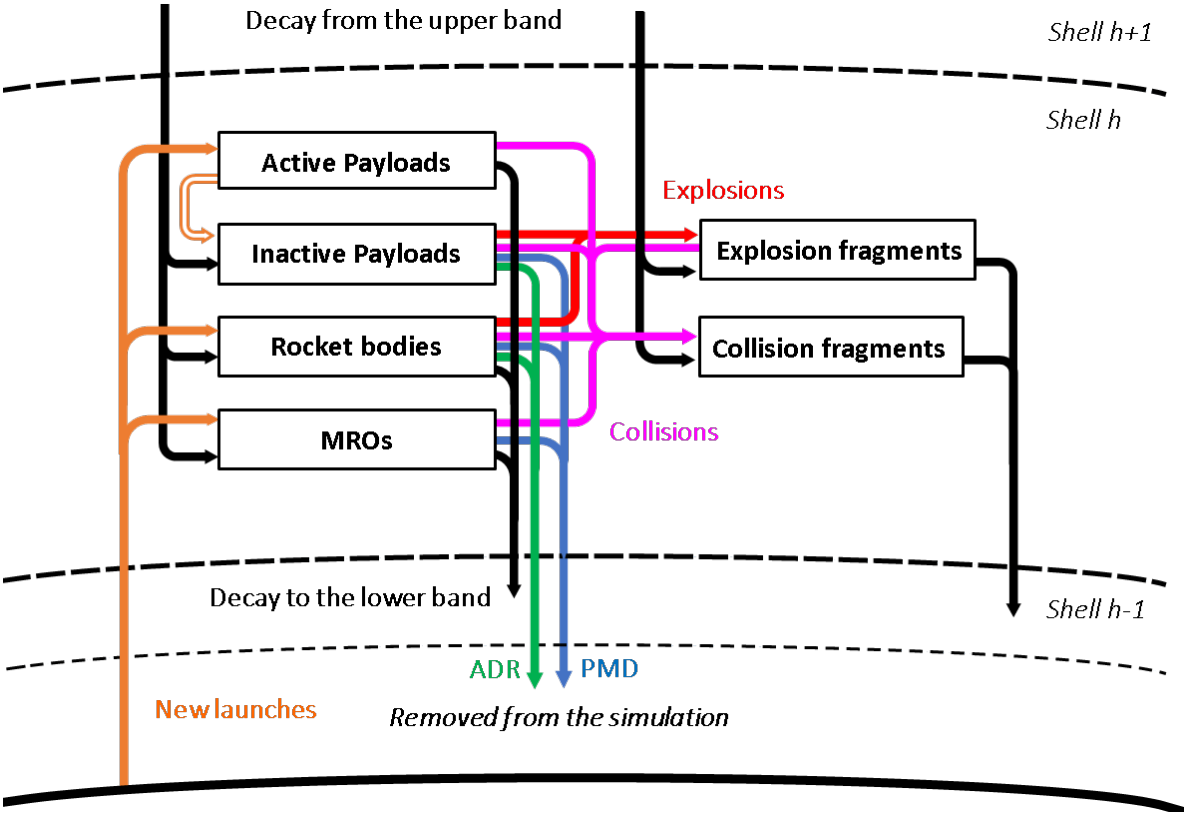

Figure 1. The schematics of object species and their interaction in MISSD. Source and sink mechanisms are depicted as inbound and outbound arrows respectively. New objects are created with launches, explosions and collisions. Conversely, removal mechanisms are the natural drag, post-mission disposal, and active debris removal.

The choice to use these six species was dictated by the goal to simulate the behaviour and the interactions (e.g. the addition, removal, and collision) of objects within and among each species based on their characteristics. Indeed, referring to Figure 1 and Eq. (6), the species interact with each other via a collision matrix. Inactive payloads and rocket bodies can also generate fragments via explosions. The launches inject only new rocket bodies, mission-related objects (MROs) and active payloads, with these latter that becomes inactive after a set lifetime period. The only natural sink effect is the natural drag which is obtained from a piecewise exponential model of the Earth's density with an 11-year solar cycle [8,9]. The model does not account for solar radiation pressure, Earth harmonics (the gravitational potential is assumed to have a spherical symmetry), luni-solar and other perturbations. Post-mission disposal is implemented in a simple way, such that satellites are removed from the same shell according to the past launch profile and a PMD compliance level parameter (from 0% to 100%). However, this simplification has the drawback of overestimating the number of inactive objects that remain for a longer period in the original shell instead of being manoeuvred into elliptic orbits or decaying in lower ones. This issue is known and will be solved in future model upgrades. It is also assumed that inactive payloads, rocket bodies and MROs are destroyed by the atmospheric drag (and removed from the simulation) within 25 years. The model is also able to perform Active Debris Removal (ADR) on inactive payloads and rocket bodies with either a constant removal rate or a rate determined by an automatic controller that simulates the human-driven interaction with the space environment. The controller can use different control laws, such as linear, quadratic and feedback ones [6,7]. Objects subject to both PMD and ADR are removed from the simulations, while in all the other cases, objects are moved among species (e.g. becoming explosion or collision fragments) or decay to the lower altitude shell due to atmospheric drag.

An initial population file generates the average physical characteristics (area, mass, radius) for each species in each altitude shell, and provides the object distribution in the various shells at the beginning of the simulation. After this stage, every object loses its identity (i.e. data on single objects is not stored) and becomes part of the data set with mean characteristics. In the same way, the mean physical features and altitude profile for launched objects are obtained from a file containing data on historical launches. The use of mean characteristics simplifies the problem and decreases computational times; however, to increase the accuracy, future model improvements will include additional discretisation on the physical parameters (e.g. with mass and area bins).

The model uses a system of nonlinear first-order differential equations to handle the population derivatives as firstly proposed in [10–12]. At every discrete time t_k, the total population $\vec{N}_T$ in each altitude spherical shell h is equal to the sum of the six object species populations $\vec{N}_y$:

$$\begin{aligned}\vec{N}_T(t_k,h) &= \sum_h \sum_y \vec{N}_y(t_k,h) \\ &= \vec{N}_{AP}(t_k,h) + \vec{N}_{IP}(t_k,h) + \vec{N}_{RB}(t_k,h) + \vec{N}_{MR}(t_k,h) + \vec{N}_{CO}(t_k,h) + \vec{N}_{EX}(t_k,h),\end{aligned} \tag{1}$$

where the subscripts AP, IP, RB, MR, CO, and EX refer respectively to the object species handled in the model, namely active payloads, inactive payloads, rocket bodies, MROs, collision and explosion fragments.

In the same way as Eq. (1), the derivative of the total population in each altitude shell is expressed as a summation of six species-related terms:

$$\begin{aligned}\dot{\vec{N}}_T(t_k,h) &= \sum_h \sum_y \dot{\vec{N}}_y(t_k,h) \\ &= \dot{\vec{N}}_{AP}(t_k,h) + \dot{\vec{N}}_{IP}(t_k,h) + \dot{\vec{N}}_{RB}(t_k,h) + \dot{\vec{N}}_{MR}(t_k,h) + \dot{\vec{N}}_{CO}(t_k,h) + \dot{\vec{N}}_{EX}(t_k,h),\end{aligned} \tag{2}$$

where each component can be cross-dependent on the population of other species, as illustrated in Figure 1. The model uses an explicit Euler model [13] to compute the future states with

$$\vec{N}(t_{k+1}) = \vec{N}(t_k) + \dot{\vec{N}}\left(t_k, \vec{N}\left(t_k\right)\right)\Delta t\,, \tag{3}$$

where, for simplicity, only the time dependency is shown, and with

$$t_{k+1} = t_k + \Delta t\,, \tag{4}$$

where Δt is small enough to prevent numerical instabilities. Each derivative in Eq. (2) is equal to the sum of six vectors,

$$\begin{aligned}\dot{\vec{N}}(t_k, h, \vec{N}(t_k, h_\eta), \dot{\vec{L}}(t)) = \dot{\vec{C}}(t_k, h_\eta, \vec{N}(t_k, h_\eta)) + \dot{\vec{D}}(t_k, h_\eta, h_{\eta+1}, \vec{N}(t_k, h_\eta)) + \\ \dot{\vec{E}}(t_k, h_\eta) + \dot{\vec{L}}(t_k, h_\eta) + \dot{\vec{M}}(t_k, h_\eta, \dot{\vec{L}}(t)) + \dot{\vec{U}}(t_k, h, \vec{N}(t_k, h_\eta)),\end{aligned} \tag{5}$$

where $\dot{\vec{C}}$ relates to collisions, $\dot{\vec{D}}$ to drag, $\dot{\vec{E}}$ to explosions, $\dot{\vec{L}}$ to launches, $\dot{\vec{M}}$ to mitigation measures, and $\dot{\vec{U}}$ to control (acting on ADR). The drag term depends on h_η and $h_{\eta+1}$, respectively the selected and the upper altitude shell, while the control can be a function of the population in multiple altitude shells. Rewriting Eq. (5) in terms of the six species and applying some assumptions (such as active payloads, MROs and collisions fragments do not explode), a system of equations is obtained:

$$\begin{cases} \dot{N}_{AP} = +\dot{C}_{AP} & & +\dot{L}_{AP} + \dot{M}_{AP} \\ \dot{N}_{IP} = +\dot{C}_{IP} + \dot{D}_{IP} + \dot{E}_{IP} & & + \dot{M}_{IP} + \dot{U}_{IP} \\ \dot{N}_{RB} = +\dot{C}_{RB} + \dot{D}_{RB} + \dot{E}_{RB} & & + \dot{L}_{RB} + \dot{M}_{RB} + \dot{U}_{RB} \\ \dot{N}_{MR} = +\dot{C}_{MR} + \dot{D}_{MR} & & + \dot{L}_{MR} + \dot{M}_{MR} \\ \dot{N}_{CO} = +\dot{C}_{CO} + \dot{D}_{CO} \\ \dot{N}_{EX} = +\dot{C}_{EX} + \dot{D}_{EX} + \dot{E}_{EX} \end{cases}, \tag{6}$$

where all the dependencies have been removed for clarity.

Note that in Eq. (6) all terms are reported with the positive sign to remain consistent with the notation used in Eq. (5). The sign of some components cannot be defined *a priori* since it usually depends on both the shell and the time. For example, the decay terms can be positive

or negative depending on the difference in the number of objects decaying from the upper shell and those decaying into the lower one. Conversely all collision and explosion terms, except for $\dot{C}_{CO}$ and $\dot{E}_{EX}$, are always negative since they remove the objects involved in fragmentation events.

3 Results and discussion

A reference case was selected to define baseline results and trends. In this way, it was possible to distinguish the effects caused by the variation of the parameters from other behaviours that are always present. Moreover, this common set of results allows a numerical comparison with respect to the sensitivity analyses performed on the launch rate and launch profile (Section 3.2 and 3.3) and on a synthetic constellation (Section 3.4).

3.1 Reference case

The reference case is a business-as-usual scenario. The initial population (and the average physical characteristics of the objects within it) were computed from 16 812 objects extracted from the MASTER 2009 dataset and split into 36 evenly spaced altitude shells (see Table 1). This study considers only objects bigger than 0.1 m and assumes that 90% of the payload objects were already inactive at the beginning of the simulation.

A mean yearly launch profile was also obtained from 491 launches in the 2009-2016 time-frame (both years included, see Figure 2 and Table 2). The projection period started in 2009 and terminated after 200 years, with an integration time step of 0.1 years. Satellites were active for 8 years before becoming inactive. Then they were removed after 25 years with a PMD compliance of 90% (and a 100% success rate). In addition, at the end-of-life, all spacecraft performed complete passivation that prevented any explosions.

Table 1. The initial population used in the base reference case and in all the following sensitivity studies.

Altitude [km]	Total Payloads	Rocket Bodies	MROs	Collision Fragments	Explosion Fragments	Total
200-250	0	2	5	6	76	89
250-300	3	2	4	6	87	102
300-350	10	3	1	3	80	97
350-400	15	6	0	6	128	155
400-450	16	8	9	5	106	144
450-500	39	19	6	6	100	170
500-550	35	23	14	4	145	221
550-600	69	33	20	12	254	388
600-650	75	73	30	24	419	621
650-700	90	25	43	25	544	727
700-750	63	21	57	38	813	992
750-800	237	84	53	72	1 392	1 838
800-850	110	58	35	57	1 230	1 490
850-900	48	40	27	61	1 340	1 516
900-950	71	31	45	50	1 029	1 226
950-1000	190	167	97	50	766	1 270
1000-1050	22	16	34	29	573	674
1050-1100	28	26	45	25	461	585
1100-1150	58	16	28	14	257	373
1150-1200	22	25	16	11	205	279
1200-1250	2	5	3	7	168	185
1250-1300	7	3	3	9	200	222
1300-1350	10	8	5	10	161	194
1350-1400	41	11	8	12	208	280
1400-1450	314	29	16	15	294	668
1450-1500	218	22	8	21	393	662
1500-1550	42	16	8	18	383	467
1550-1600	12	43	7	16	268	346
1600-1650	7	6	4	16	196	229
1650-1700	9	4	1	9	189	212
1700-1750	0	3	3	9	108	123
1750-1800	3	3	0	2	81	89
1800-1850	1	0	0	2	49	52
1850-1900	1	0	1	3	27	32
1900-1950	1	1	1	0	39	42
1950-2000	0	3	1	3	45	52
Total	1 869	835	638	656	12 814	16 812

Table 2. The total number of launches in the 2009-2016 time-frame (both years included).

Altitude [km]	Active Payloads [#/yr.]	Rocket Bodies [#/yr.]	MROs [#/yr.]	Total launches [#/yr.]
200-250	1	2	1	4
250-300	9	1	0	10
300-350	3	1	1	5
350-400	5	1	1	7
400-450	8	6	4	18
450-500	28	11	6	45
500-550	13	16	3	32
550-600	25	8	6	39
600-650	47	12	12	71
650-700	52	7	9	68
700-750	24	5	4	33
750-800	15	6	5	26
800-850	15	7	6	28
850-900	8	2	1	11
900-950	10	4	2	16
950-1000	11	8	3	22
1000-1050	2	1	9	12
1050-1100	1	2	0	3
1100-1150	3	1	3	7
1150-1200	0	1	3	4
1200-1250	0	1	0	1
1250-1300	0	0	0	0
1300-1350	2	1	0	3
1350-1400	0	0	0	0
1400-1450	8	2	0	10
1450-1500	10	3	1	14
1500-1550	0	0	0	0
1550-1600	0	0	0	0
1600-1650	0	0	0	0
1650-1700	1	1	0	2
1700-1750	0	0	0	0
1750-1800	0	0	0	0
1800-1850	0	0	0	0
1850-1900	0	0	0	0
1900-1950	0	0	0	0
1950-2000	0	0	0	0
Total	301	110	80	491

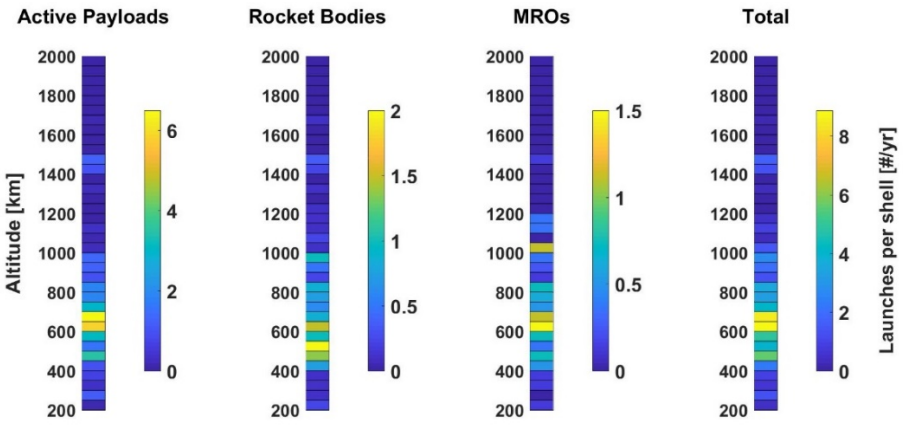

Figure 2. Distribution of yearly launches as function of the altitude shell and species.

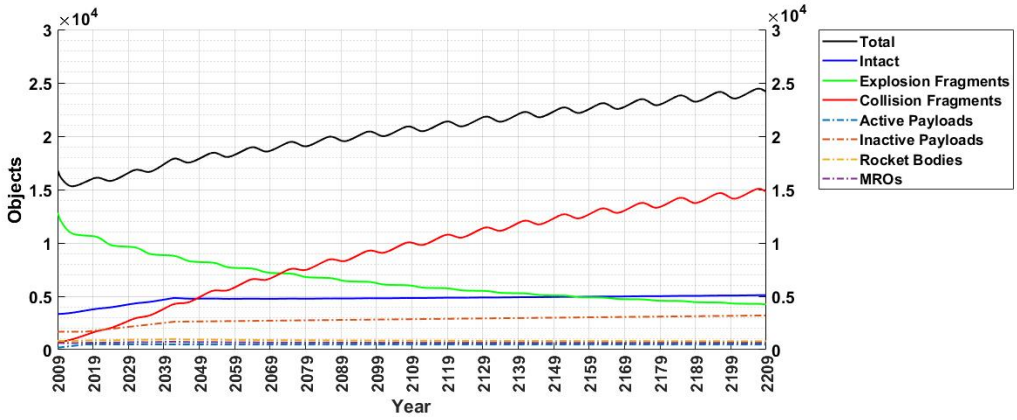

Figure 3. The evolution of the total number of object in LEO for each species in the reference case.

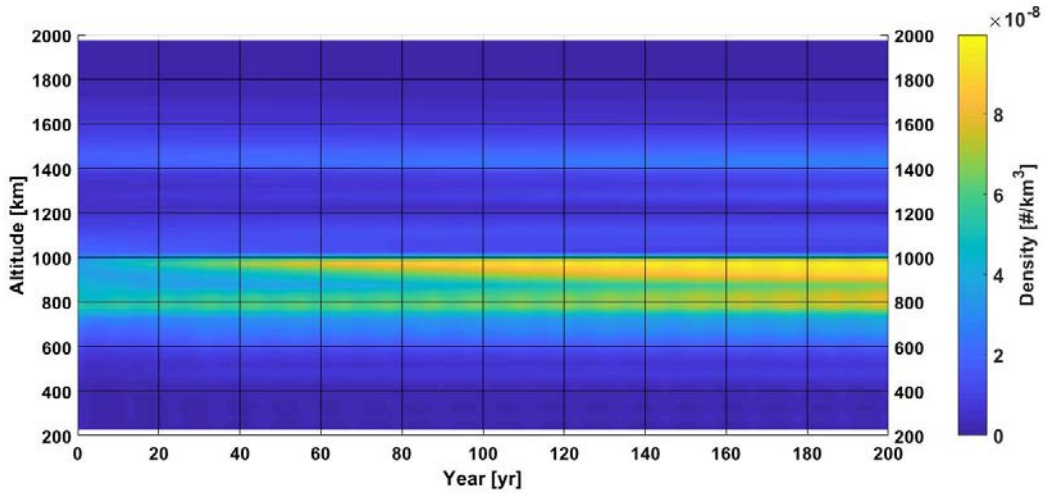

Figure 4. The evolution of the total spatial density in the reference case. The two regions with the higher values have the two inner boundaries that tend to get closer over time.

Table 3. The orbital population of the six species in the reference case at the initial and end time. Collision fragments are the main contributor to the total population.

Object species	Population at the initial time	Population at the end time	Variation w.r.t the initial population [%]
Intact objects	3 342	5 103	+152.7
Active Payloads	187	480	+156.8
Inactive Payloads	1 682	3 203	+90.4
MROs	835	789	-5.5
Rocket Bodies	638	631	-1.1
Collision fragments	656	14 793	+2 155.0
Explosion fragments	12 814	4 243	-66.9
Total	16 812	24 139	+43.6

The evolution of the orbital population for each species and total spatial density are depicted respectively in Figure 3 and Figure 4, while numerical data are listed in Table 3. The choice to investigate the spatial density (instead of the orbital population) was driven by the fact that, in the model, the orbital collision rate has a quadratic dependence on the spatial density. Therefore, peaks in the density reflect higher collision rates and thus generate more collision fragments. Note that the solar cycle caused periodic ripples in the population and therefore, even when using a monotonic unmodulated trend (i.e. removing the ripples), the measured values might not assume the maximum (or the minimum) value at the end time (see Figure 3). This behaviour also occurred in the following results and will be further omitted.

The major density peak at the beginning of the projection period lies at the altitude of 750-800 km. With time, it increases in magnitude to a plateau that extends upwards up to the 850-900 km shell (Figure 4). A new trend emerges over time with an absolute maximum value of 1.02×10^{-7} objects/km^3 in the 900-1000 km region. Here the beneficial effect of the atmospheric drag is weaker than at lower altitudes. In addition, continuous launches to the 900-1050 km region contributed to the formation of a new high-density peak-region. These objects remained

in the environment for a longer time but eventually decayed, forming a high-density region that expanded downwards toward 900 km, almost merging with the previous region.

A third region lies in 1400-1550 km, as depicted in Figure 5. Here, in the mid-1970s, the second stages of three Delta rockets exploded. The generated cloud of debris will remain at these altitudes due to the negligible effect of drag.

An insight into the evolution of the spatial density of the single species is given in Figure 5. Each graph has a different density scale to enhance the trends present in each species. In general, the values can be one or two orders of magnitude smaller than the total spatial density (which is depicted in Figure 4). Comparing Figure 2 with Figure 5, active payloads, rocket bodies and MROs tend to accumulate in those shells where there are more launches. However, the dynamics of the total density is composed of collision fragments and, in a minor way, by inactive payloads.

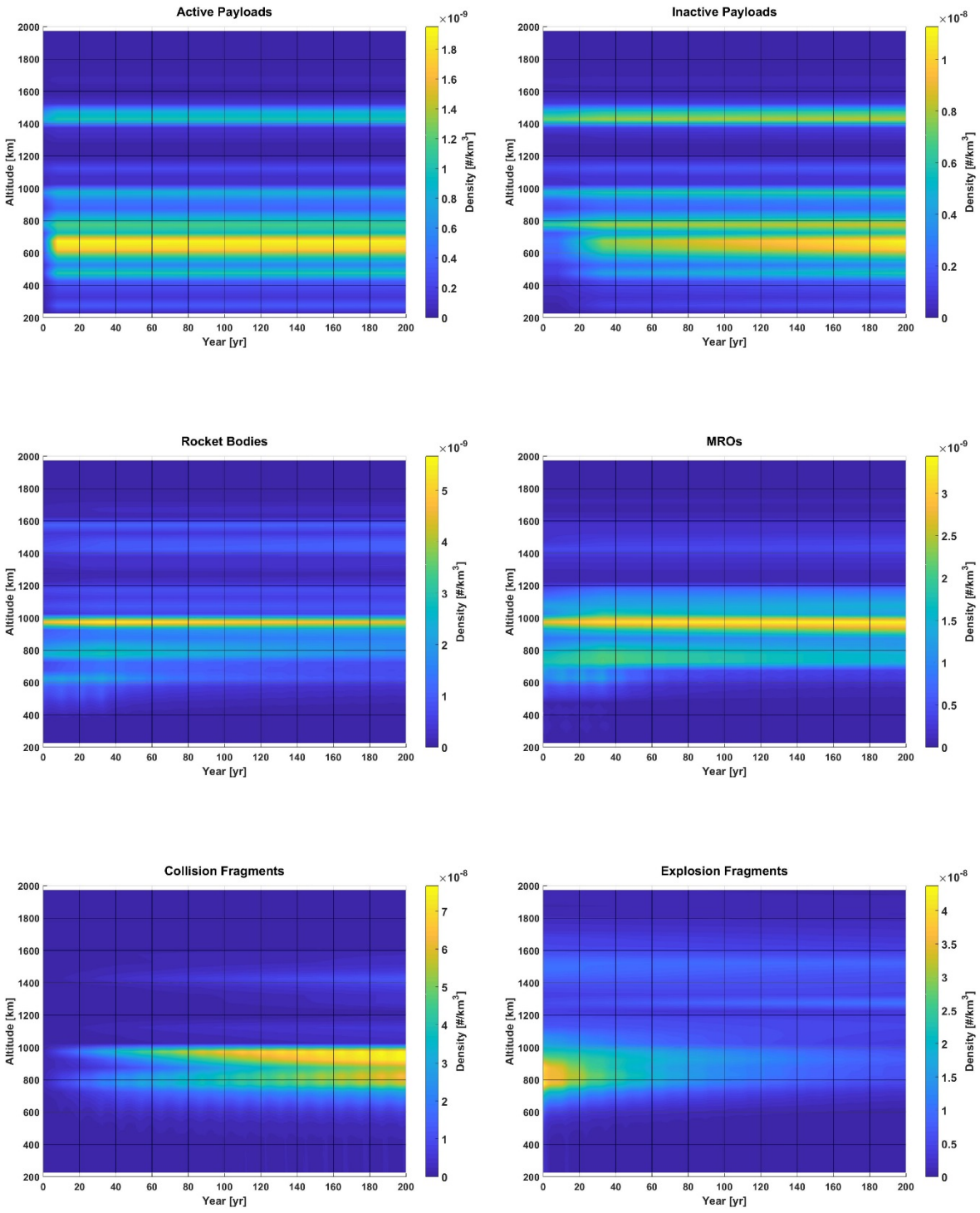

Figure 5. The evolution of orbital density for each species. Values are interpolated from those computed at the middle point of each shell. Different colour scales are used to enhance trends in each species.

Rocket bodies and MROs have a similar graph; their density remains in both cases almost constant during the whole simulations due to the quasi-equilibrium of new launches performed with decayed objects. The active payloads also have a similar plot; however, their amount increases due to the accumulation in the first years of the simulation. This increase stops when the first payloads start to be moved into the inactive species, reaching a new equilibrium with the new payloads launched. The same accumulation phenomenon occurs in the inactive species. Here the process only starts after the first payloads become inactive (i.e. after 8 years) and continues for 25 years. Then the trend reduces its rate because the inactive payloads begin to be removed from the simulations. However, 10% of them are not compliant with PMD measures and accumulate over time. In contrast, explosion and collision fragments have different trends. The former decay over time because there are no new explosions, while the latter increase over the timeframe. As previously stated in Section 2, the simple approach for removing objects after their end-of-life generates inactive objects (and thus collision fragments) that remain in the same shell of launch for a longer period instead of being spread over multiple shells at lower altitudes.

3.2 Sensitivity to the launch rate

In this analysis, four scenarios were compared to the reference case which had a launch rate defined as $L_0 \triangleq L(t,h)$.. The four cases were: no-launches, half the reference launch rate, i.e. $0.5L_0$, one-and-one-half times the launch rate, i.e. $1.5L_0$, and twice the launch rate, i.e. $2.0L_0$. The simulation parameters are the same of the reference case (including the PMD compliance for all intact objects set to 90%). Figure 6 illustrates the evolution of the population at the end of the projection period for each scenario respectively, while Table 4 lists the numerical results.

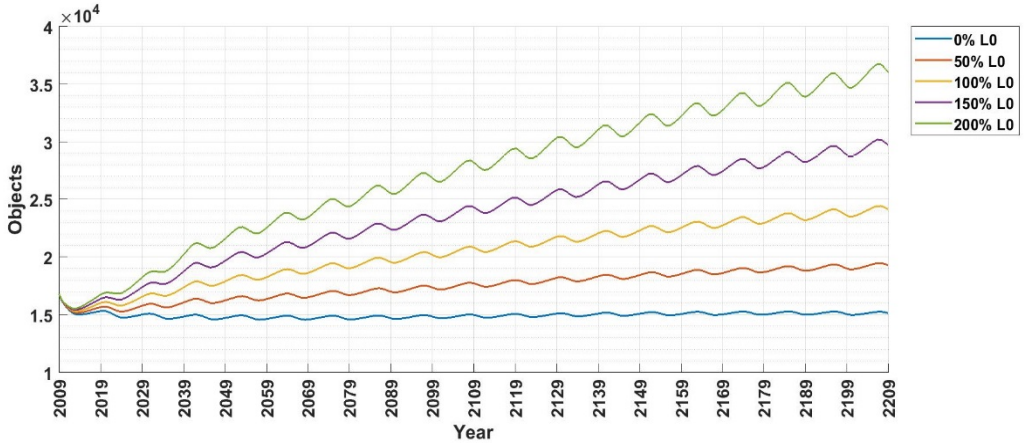

Figure 6. Comparison of the total end population for various multipliers of the base launch profile $L_0(h)$. *The population decreases only with no new launches (*$0\%L_0$*)*

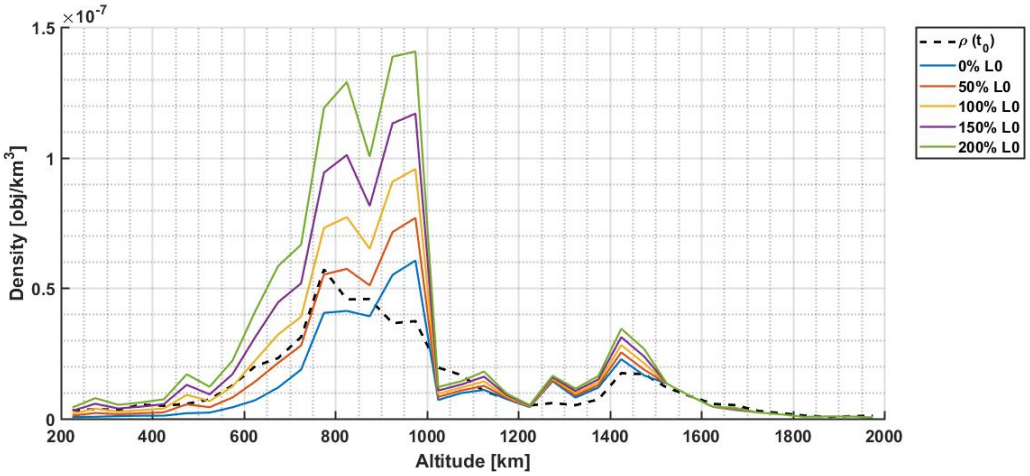

Figure 7. In several shells, the spatial density assumes values higher than the initial one for all the multipliers of the base launch profile L_0.

The no-launches scenario was the most optimistic case, and it revealed a peak in spatial density in the 900-1000 km region. Indeed, even though this was the only case in which the final total population was smaller than the initial population (-9.9%), the spatial density reached values higher than the initial one in several shells (Figure 7). A behaviour similar to the reference case was also observed in the other cases, with increasing density values, with a plateau in the 750-850 km region and attaining the absolute maximum value in the 950-1000 km region. In

the region of 1400-1500, the maximum spatial density increased with the number of launches as well, but it always assumed values smaller than 0.5×10^{-7} objects/km^3.

Table 4. The numerical results of the sensitivity study on the launch rate. The third case corresponds to the reference one. The maximum density (achieved among all altitude shell) always happens in the 950-1000 km shell.

	Total end population	Total collisions	Maximum density [#/km^3]	Time of maximum density [yr.]	Maximum density at end time [#/km^3]
No launches	15 147	35.16	6.91 x10^{-8}	2107	6.06 x10^{-8}
$0.5L_0$	19 295	51.33	8.20 x10^{-8}	2140	7.69 x10^{-8}
$1.0L_0$	24 139	73.73	9.87 x10^{-8}	2173	9.57 x10^{-8}
$1.5L_0$	29 713	103.32	1.20 x10^{-7}	2206	1.17 x10^{-7}
$2.0L_0$	36 050	141.17	1.44 x10^{-7}	2207	1.41 x10^{-7}

Concerning the population evolution, the results in Table 4 suggest that the number of objects in the final population and the number of collisions are not linearly proportional to the launch rate parameter. Indeed, when extending the simulations up to a ten-fold increase in the launch activity ($10L_0$), a non-linear trend emerged (Figure 8) due to an increasing number of both targets and newly generated fragments that act as projectiles.

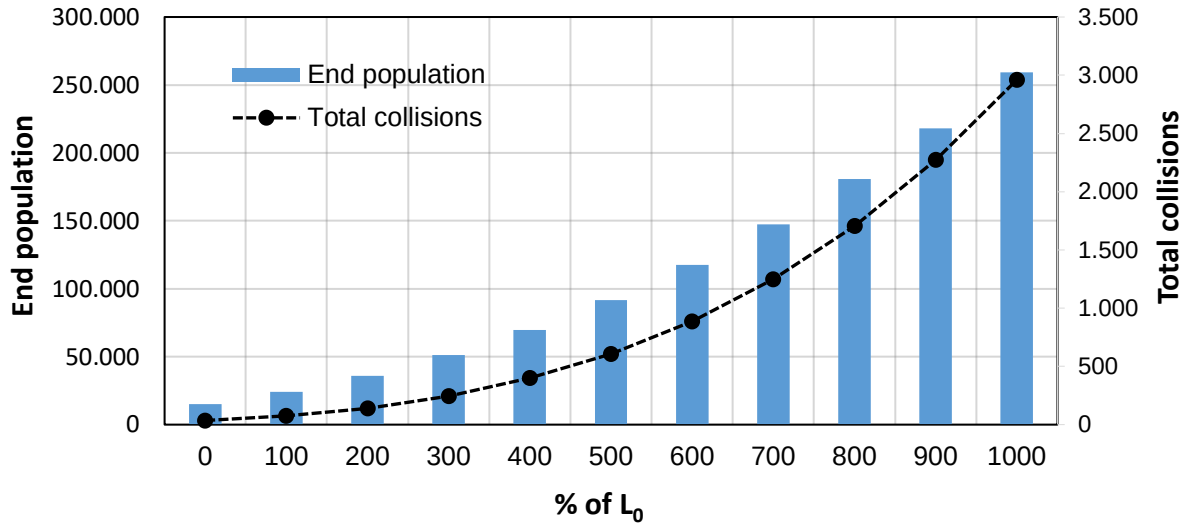

Figure 8. The non-linear relationship among the launch rate, the end population, and the total cumulative number of collisions for an extended set of simulations (up to a ten-fold increase in the launch activity).

3.3 Sensitivity to the launch altitude profile

A second study was performed to estimate how many additional spacecraft could be supported by the environment before exceeding, after 200 years, a density threshold of 10^{-7} objects/km^3, equivalent to 100 objects in a cube with a side of 1000 km. This threshold was chosen due to its proximity to the maximum density reached at the end time of the reference case, equal to 9.57×10^{-8} objects/km^3. This study could then provide an indication of the size of a satellite constellation or how large could be the increase in launch activity before generating a collision risk (in a specific region) similar to the maximum achieved in the reference case.

For each altitude shell, simulations were run with a trial and error method until the threshold was exceeded (at the end time) in the same shell in which the payloads were launched (the solid black line in Figure 9) or until the threshold was exceeded in any other shell (the dotted blue line). In this latter case the passing of the threshold is caused by fragments decaying from the shell with additional launches.

For altitudes lower than 750 km, the natural drag prevented the build-up of the population even with more collisions occurring at these low altitudes. In the region of 750-1000 km lie the lower points of the curve, with values from one to six additional objects launched per year. Several local minima lie between 1100 and 1300 km, with values that range between 6 and 21 objects/year.

Taking a broader view, the blue curve in Figure 9 is always equal or lower to the black one. Indeed, different results are obtained when launching additional objects in shells from 1000 to 1200 km, with as low as just three additional launches. In these cases, the fragments generated from collisions in the shell with the additional launches decay in the lower shells, some of which have higher spatial densities. In particular, the threshold was always exceeded in the 950-1000 km shell.

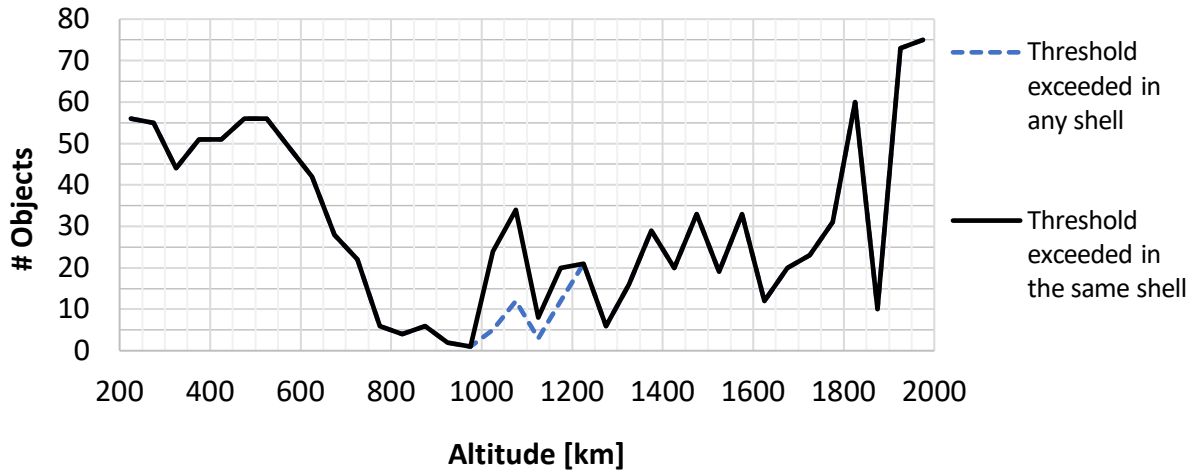

Figure 9. The minimum number of additional launched payloads to reach the density of 1×10^{-7} *objects per square kilometre in the same shell (solid line) or in any other shell (dashed line) with respect to where the additional payloads were launched. The lower values are assumed between 750 and 1300 km.*

As shown by the dotted line in Figure 7, existing congestion is found between 700-1000 km and 1400-1500 km. Instead, the regions that require the lower additional number of launches to reach the selected threshold are between 750 and 1300 km. Above 1300 km, the minimum

number of objects needed to reach the threshold density tends to increase, and the threshold is always reached in the same shell in which the launches occur. At these altitudes, the atmospheric drag is negligible, while the growth in the shell volume (the upper shell was 1.58 times the lower one) helped to decrease the density and the collision risk, and therefore increase the slope of the curve. The resulting differences in values among neighbouring shells were significant (up to 63 objects between the 1800-1850 km and 1850-1900 km shells). This is due to the difference in the assumed mean values of the physical characteristics in each shell, especially of the radius and mass (which determines the collision rate and the number of generated fragments respectively). This known limitation could be addressed with the addition of a discretisation of the radius and mass in multiple bins.

The initial population had very few objects in the upper shells, with only 22 intact objects above 1700 km (as listed in Table 1). This lack of data results in very poor statistical values of mean physical features. In the extreme case of no object present in a shell, a medium value was computed between the shells immediately above and below .

3.4 Large constellation

Several companies, including OneWeb, Boeing, SpaceX and Samsung, have recently shown interest in the 1100-1300 km region, proposing constellations of hundreds (or even thousands) of spacecraft to provide telecommunications services and global internet coverage with a low latency [3,14]. On the 22nd of February 2018, SpaceX successfully launched the first two test satellites of their Starlink constellation, receiving the Federal Communication Commision authorisation to launch and operate a total of 4 425 satellite in LEO [15]. In addition, OneWeb stated that 10 test satellites (supposed to be launched in May 2018) will be launched by the end of 2018, while commercial service will start in 2019[16]. This section presents a study, similar to [4], where additional active payloads are launched in the 1200-1250 shell to simulate

synthetic constellations of different size or with different residual post-mission times. All the tests start in 2009 with the same initial population and launch profile of the reference case in Section 3.1. The constellation is active for 50 years from 2020 to 2070 and becomes fully deployed in 2025, with the same launch rate used to build-up and to replenish the constellation. After 5 years of operative life, satellites become inactive (also those not belonging to the constellation), and 90% of them are removed from the environment accordingly to the set post-mission lifetime.

In the simulation, constellation satellites were assumed to have a mass of 200 kg and a size of 1 m. In this way, they are similar to those proposed for the planned constellations that should have a mass 150-200 kg and an approximate volume of $1m^3$ (with folded solar panels) [16,17].

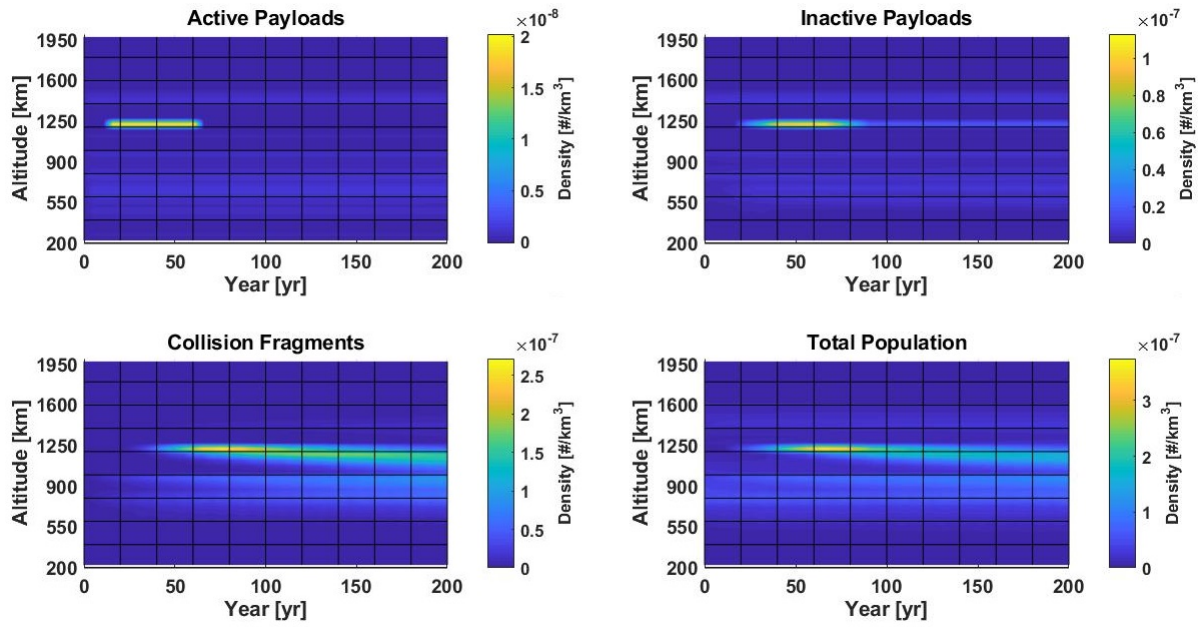

Figure 10. The spatial density of active and inactive payloads, collision fragments and total population as function of altitude and time with a constellation formed by 750 satellites.

3.4.1 Sensitivity to constellation size

Different constellation sizes were tested, launching up to 8 rocket each with 25 satellites (these values are compatible with the proposed plans and payload capability of commercial rocket launchers). Therefore, up to 200 satellites were launched per year, forming constellations of 250, 500, 750, and 1000 units in a maximum time of 5 years. Each of them had an operational life of 5 years and 25 years of residual lifetime.

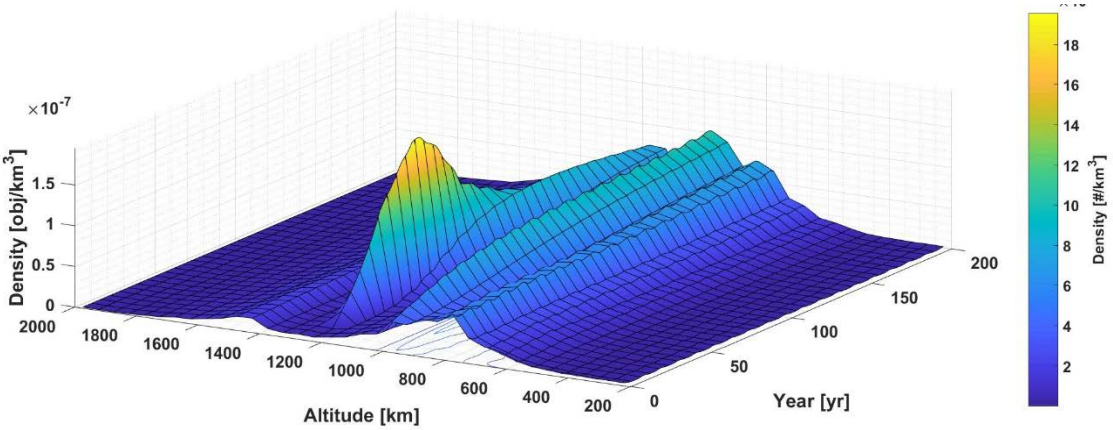

Figure 11. The total spatial density as function of altitude and time with a constellation formed by 500 satellites with 5 years of operative life and 25 years of post-mission residual lifetime.

With 500 or more satellites, the maximum density is achieved in the constellation shell just after the constellation decommissioning (see Figure 11). Conversely, with 250 satellites, the density peak remains in the lower, more crowded 950-1000 km region. In this case, both the collisions and the total population at the end time remain relatively close to the case with no constellation with an increase of +7.62% and +9.94% respectively (Table 5). The evolution of the density of the 500-satellite constellation has a particular feature: the peak density is in the 1200 km region in 2074, but then the effects of the constellation presence vanish with time. Indeed, at the end time, the maximum density occurs (like in the no-constellation case) in the 950-1000 km shell.

Table 5. The total end population and the cumulative collisions increase with the constellation size. The first row represents a benchmark no-constellation scenario.

Constellation size	Total end population	Total collisions
0	22 353	64.96
250	24 568	69.91
500	30 354	89.94
750	39 928	138.25
1000	53 394	233.34

Table 6. The maximum density increases with the constellation size.

	Maximum density during the simulation			Maximum density at end time	
Constellation size	Value [#/km^3]	Time [yr.]	Altitude [km]	Value [#/km^3]	Altitude [km]
0	9.55×10^{-8}	2162.0	950-1020	9.23×10^{-8}	950-1000
250	9.72×10^{-8}	2206.0	950-1000	9.98×10^{-8}	950-1000
500	1.95×10^{-7}	2074.0	1200-1250	1.03×10^{-7}	950-1000
750	3.75×10^{-7}	2074.6	1200-1250	1.56×10^{-7}	1150-1200
1000	6.17×10^{-6}	2075.1	1200-1250	2.72×10^{-7}	1150-1200

The constellation satellites in the real world should be transferred (at the end of their operative life) to an elliptic disposal orbit with a much lower perigee. Therefore, inactive payloads and collision fragments should not amass in a thin region but spread to lower altitudes and decay faster. As a result, MISSD overestimates the number of collision fragments and the total population.

3.4.2 Sensitivity to residual lifetime

This study tested the sensitivity of the LEO population to the post-mission residual orbital time. A constellation of 750 satellites was built up and maintained with 150 satellites launched per year (via 6 launches with 25 satellites each) in the 1200-1250 km shell with a residual lifetime of 0, 5, 10, 15, 20, and 25 years after 5 years of operative life.

Table 7. The total end population and the cumulative collisions increase with the residual lifetime.

Residual lifetime	Total end population	Total collisions
0	21 246	50.03
5	23 666	59.13
10	26 816	71.87
15	30 629	88.95
20	35 025	110.92
25	39 928	138.25

Table 8. The maximum density increases with the residual lifetime.

	Maximum density during simulation			Maximum density at the end time	
Residual lifetime	Value [#/km^3]	Time [yr.]	Altitude [km]	Value [#/km^3]	Altitude [km]
0	7.81 x10^{-8}	2206.0	950-1000	7.64 x10^{-8}	950-1000
5	1.09 x10^{-7}	2070.1	1200-1250	8.26 x10^{-8}	950-1000
10	1.64 x10^{-7}	2070.1	1200-1250	8.98 x10^{-8}	950-1000
15	2.27 x10^{-7}	2074.0	1200-1250	9.80 x10^{-8}	950-1000
20	2.99 x10^{-7}	2074.6	1200-1250	1.20 x10^{-7}	1150-1200
25	3.75 x10^{-7}	2162.0	1200-1250	1.56 x10^{-7}	1150-1200

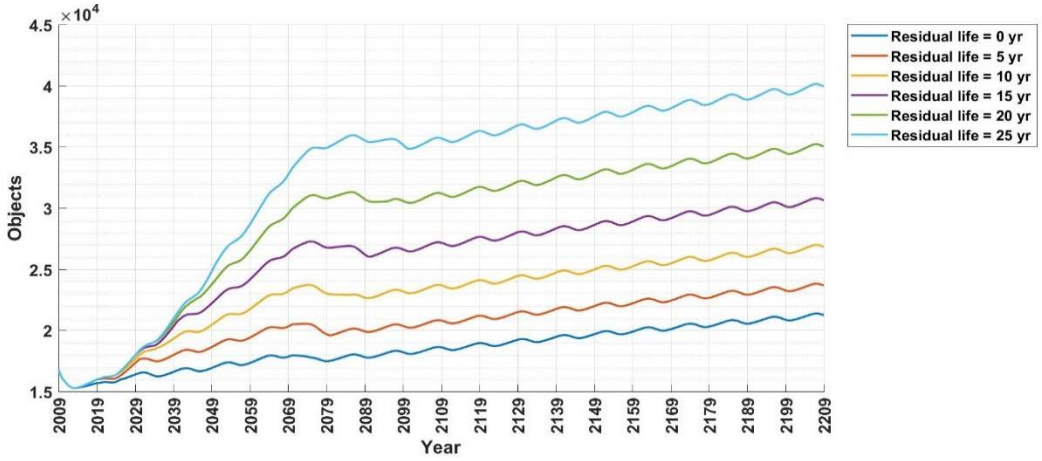

Figure 12. The evolution of the total LEO population as function of the satellite residual orbital life.

Results show that the residual lifetime influences the density, and thus the collision rate and total population (Table 7) at the constellation altitude and in the lower ones (Table 8). Indeed, fewer inactive payloads result in a lower number of collisions, leading to a beneficial effect visible from the very early phase of the constellation build-up (Figure 12). The constellation presence and its orbital lifetime produced only a temporary effect, as also highlighted in [4]. However, after the decommissioning of the constellation, ranging from 2070 to 2095, the total population always increases with similar linear trends (Figure 12).

Compared to the case with 25 years, when selecting 5 years of residual lifetime, the total end population and the number of collisions decreased by 40.7% and by 57.2% respectively. This latter case is of particular interest, being similar to planned constellations that should perform end-of-life manoeuvres to move the satellite to a highly elliptic orbit with less than 5 years of orbital lifetime [14]. In this aspect MISSD differs since it computes the drag as for a circular orbit and maintains the inactive payload in the original orbit, thereby it overestimates the number of inactive payloads and collisions. Once these aspects have been considered, the LEO population size should assume a lower value. The current model applies the same selected residual lifetime to all the rocket bodies, MROs, and inactive payloads (belonging both to

constellation or not). Therefore, the model underestimates these populations except when the selected residual life corresponds to the default value of 25 years. In this case, the total population increases by 65.4% from about 24 000 (of the reference case) to 39 000, while collision grew by 87.5% from 74 to 138 (Table 7).

4 Conclusions

Several studies were performed using the MISSD model to test the sensitivity of the LEO population to the launch rate and launch profile, and to investigate the effect of the size and residual lifetime of a large constellation of spacecraft in the 1200-1250 km region.

The results suggested that three regions are particularly critical in LEO. The first one lies at 750-850 km, where today's debris population causes a future increase in spatial density. The lowest part of this region reached a population size and spatial density lower than the initial ones only in the extreme case of completely stopping the launch activity and using for all the existing intact objects a 90% compliance with post-mission mitigations guidelines. The second region lies at 900-1000 km, where currently a high number of big and massive objects reside. Here drag is not sufficient to maintain a balance between injected and decaying objects even in the no-launch scenario. Moreover, the spatial density of this region increases over time, becoming the highest in LEO. The third region extends from 1100 to 1300 km. Here the initial population is low, but the effect of drag is negligible. Therefore, presuming that no additional mitigation measures are taken, any additional object that reaches orbit in this region contributes to the build-up of the orbital population. With an increase as low as six more spacecraft per year, the spatial density of this region reaches the same maximum values obtained in the business-as-usual case at the end time.

The launch of a large constellation of 250 or more satellites at 1200-1250 km altitude could increase the collision risk in LEO, especially in the 1100-1250 km region. However, reducing

the residual lifetime from 25 to 5 years could prevent the increase of the inactive population in the early phase of the constellation build-up, leading to a beneficial effect due to the prevention of collision fragments. The simulations use a very optimistic value for PMD compliance, which however corresponds to the current target value. On the other hand, MISSD overestimates the number of fragments generated by the fragmentation of inactive constellation spacecraft. Nevertheless, the results should be taken as a warning of the criticality of the 1000-1300 km region. Moreover, the simulated scenarios are similar in number and physical characteristics to some of the recently proposed large constellations. Considering the results, commercial operators should commit to the design of their spacecraft so to have the lowest residual life and to maximise the satellite deorbit reliability. Such measures could lead to mitigating the possible increase in the orbital population and collision risk caused by the presence of large constellations in LEO.

Acknowledgements

The Doctoral Training Partnership funded part of this work through the Engineering and Physical Sciences Research Council (grant EP/M50662X/1). The ESA Space Debris Office provided data on the orbital population and launch traffic.

References

[1] C. Pardini, L. Anselmo, Review of past on-orbit collisions among cataloged objects and examination of the catastrophic fragmentation concept, Acta Astronaut. 100 (2014) 30–39. doi:10.1016/j.actaastro.2014.03.013.

[2] J.C. Dolado-Perez, C. Pardini, L. Anselmo, Review of the uncertainty sources affecting the long-term predictions of space debris evolutionary models, Acta Astronaut. 113 (2015) 51–65. doi:10.1016/j.actaastro.2015.03.033.

[3] J. Radtke, C. Kebschull, E. Stoll, Interactions of the space debris environment with mega constellations - Using the example of the OneWeb constellation, Acta Astronaut. 131 (2017) 55–68. doi:10.1016/j.actaastro.2016.11.021.

[4] B. Bastida Virgili, J.C. Dolado-Perez, H.G. Lewis, J. Radtke, H. Krag, B. Revelin, C. Cazaux, C. Colombo, R. Crowther, M. Metz, Risk to space sustainability from large constellations of satellites, Acta Astronaut. 126 (2016) 154–162. doi:10.1016/j.actaastro.2016.03.034.

[5] C.R. Boshuizen, J. Mason, P. Klupar, S. Spanhake, Results from the Planet Labs Flock Constellation, 28th Annu. AIAA/USU Conf. Small Satell. (2014) SSC14-I-1.

[6] G.L. Somma, H.G. Lewis, C. Colombo, Adaptive remediation of the space debris environment using feedback control, in: 67th Int. Astronaut. Congr., Guadalajara, Mexico, 2016. https://eprints.soton.ac.uk/403265/ (accessed April 7, 2017).

[7] G.L. Somma, C. Colombo, H.G. Lewis, A Statistical LEO Model to Investigate Adaptable Debris Control Strategies, in: T. Flohrer, F. Schmitz (Eds.), 7th Eur. Conf. Sp. Debris, ESA Space Debris Office, Darmstadt, Germany, 2017.

[8] D.G. King-Hele, Satellite Orbits in an Atmosphere: Theory and Application, Blackie and Son Ltd., Glasgow, U.K., Glasgow, 1987.

[9] D.A. Vallado, Fundamentals of Astrodynamics and Applications, 4th ed., Microcosm Press and Springer, Hawthorne, CA, 2013.

[10] D.L. Talent, Analytic Model for Orbital Debris Environmental Management, J. Spacecr. Rockets. 29 (1992) 508–513. doi:10.2514/3.25493.

[11] P. Farinella, A. Cordelli, The Proliferation of Orbiting Fragments: a Simple Mathematical Model, Sci. Glob. Secur. 2 (1991) 365–378. doi:10.1080/08929889108426373.

[12] A. Rossi, A. Cordelli, P. Farinella, L. Anselmo, Collisional evolution of the Earth's orbital debris cloud, J. Geophys. Res. 99 (1994) 23,195-23,210. doi:10.1029/94JE02320.

[13] H.G. Lewis, G.G. Swinerd, R.J. Newland, A. Saunders, The fast debris evolution model, Adv. Sp. Res. 44 (2009) 568–578. doi:10.1016/j.asr.2009.05.018.

[14] M. Lindsay, OneWeb – Overview, in: 53rd Sess. Sci. Tech. Subcomm. UNCOPOUS, Wien, Austria, 2016: pp. 1–18.

[15] Federal Communication Commision, FCC authorizes SpaceX to Provide Broadband Services via Satellite Constellation, FCC News from Fed. Commun. Commision. (2018). https://transition.fcc.gov/Daily_Releases/Daily_Business/2018/db0329/DOC-349998A1.pdf (accessed May 30, 2018).

[16] OneWeb, OneWeb Satellites Breaks Ground On The World' s First State-Of-The-Art High-Volume Satellite Manufacturing Facility, Press Release. (2017).

http://oneweb.world/press-releases/2017/oneweb-satellites-breaks-ground-on-the-worlds-first-state-of-the-art-high-volume-satellite-manufacturing-facility (accessed September 4, 2017).

[17] T. Azzarelli, Future connectivity via LEO satellites, in: TechUK, London, United Kingdom, 2015: pp. 1–10.

Vitae

Gian Luigi Somma achieved a MEng in Astronautical Engineering at the School of Aerospace Engineering, University of Rome La Sapienza. During his career, he worked as a thermal, mechanical, and system engineer within ESA, DLR, and currently for the first CubeSat of the University of Southampton (University of Southampton Small Satellite, UoS3). Member of the Royal Aeronautical Society, Gian Luigi is a Ph.D. Fellow in the Astronautics Research Group at the University of Southampton where he researches on space debris modelling and mitigation.

Hugh G. Lewis gained a Masters degree in Control Systems from the University of Sheffield in 1993 and a Ph.D. in Remote Sensing from the University of Southampton in 1998. Today, he is a Senior Lecturer in Aerospace Engineering at the University of Southampton and leads the Astronautics Research Group's space debris activities. He is a member of the UK Space Agency delegation to the Inter-Agency Space Debris Coordination Committee (IADC) and the Space Missions Planning Advisory Group, and he is also a member of the UK delegation to the United Nations Committee on the Peaceful Uses of Outer Space.

Camilla Colombo is Associate Professor at the Department of Aerospace Science and Technology of Politecnico di Milano, where she leads a European Research Council Starting Grant 2016-2020. Her work, published in 35 journal papers and 100 conference publications, spans orbital dynamics, space debris, trajectory design and control, and asteroid deflection. She is involved in the European Commission funded project ReDSHIFT and in contracts funded by the European Space Agency. Between 2012 and 2016, she was Associate Professor at the University of Southampton. Previously, she worked as a Research Fellow at the Politecnico di Milano, and at the University of Strathclyde, and as a Research Associate at the University of Glasgow. Camilla received her PhD from the University of Glasgow in 2010 and MEng in Aerospace Engineering from Politecnico di Milano in 2005.